Article

Analysis of Coiled-Coil Interactions between Core Proteins of the Spindle Pole Body

Nora Zizlsperger, Vladimir N. Malashkevich, Shirin Pillay, and Amy E. Keating

Biochemistry, **2008**, 47 (45), 11858-11868• DOI: 10.1021/bi801378z • Publication Date (Web): 14 October 2008

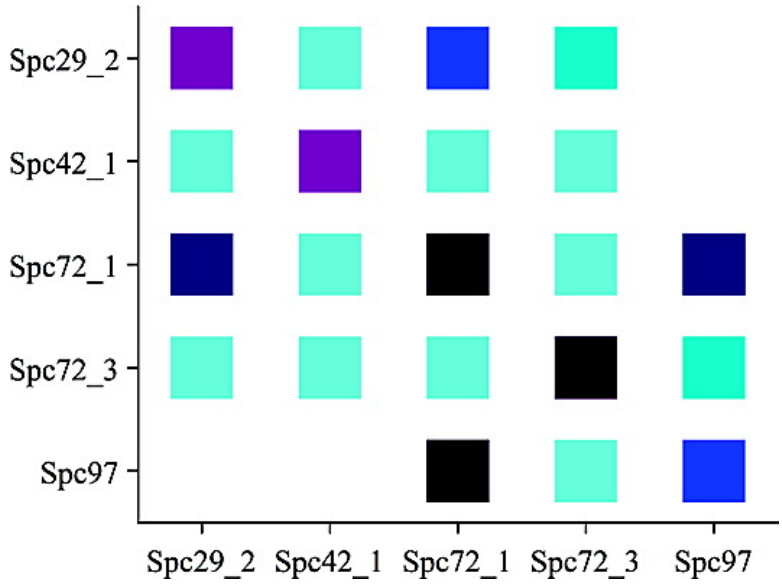

Analysis of Coiled-Coil Interactions between Core Proteins of the Spindle Pole Body[†,‡]

Nora Zizlsperger, Vladimir N. Malashkevich,[§] Shirin Pillay, and Amy E. Keating*

Department of Biology, Massachusetts Institute of Technology, 77 Massachusetts Avenue, Cambridge, Massachusetts 02139

Received July 23, 2008; Revised Manuscript Received September 4, 2008

ABSTRACT: The spindle pole body (SPB) is a multiprotein complex that organizes microtubules in yeast. Due to its large size and association with the nuclear membrane, little is known about its detailed structure. In particular, although many SPB components and some of the interactions between them have been identified, the molecular details of how most of these interactions occur are not known. The prevalence of predicted coiled-coil regions in SPB proteins suggests that some interactions may occur via coiled coils. Here this hypothesis is supported by biochemical characterization of isolated coiled-coil peptides derived from SPB proteins. Formation of four strongly self-associating coiled-coil complexes from Spc29, Spc42, and Spc72 was demonstrated by circular dichroism (CD) spectroscopy and a fluorescence resonance energy transfer (FRET) assay. Many weaker self- and heteroassociations were also detected by CD, FRET, and/or cross-linking. The thermal stabilities of nine candidate homooligomers were assessed; six unfolded cooperatively with melting temperatures ranging from <11 to >50 °C. Solution studies established that coiled-coil peptides derived from Spc42 and Spc72 form parallel dimers, and this was confirmed for Spc42 by a high-resolution crystal structure. These data contribute to a growing body of knowledge that will ultimately provide a detailed model of the SPB structure.

The spindle pole body (SPB)[1] is the microtubule organizing center of *Saccharomyces cerevisiae* (*1, 2*). This large multiprotein complex functions to coordinate and nucleate both nuclear and cytoplasmic microtubules and is necessary for chromosome segregation, nuclear positioning, and karyogamy. Electron microscopy and tomography experiments have provided a low-resolution structure of the SPB (*3*−*5*), showing a multilayered short cylinder spanning the nuclear membrane with cytoplasmic and nuclear microtubules connected to the outer and inner layers, respectively. A "half-bridge" structure, located on one side of the SPB and within the nuclear membrane, serves as the site of SPB duplication. Genetic and biochemical studies have identified approximately 20 proteins that comprise the SPB complex (*1, 6*−*8*). Using immuno-EM, proteins have been localized to regions of the SPB (core, membrane-associated, half-bridge) or particular layers or plaques of the SPB core (outer, intermediate 1, intermediate 2, central, inner) (*6, 9*) (Figure 1). Given the low diversity of proteins comprising the SPB, up to 1000 copies of each are required for assembly of the ∼300−500 MDa complex (*1, 7*).

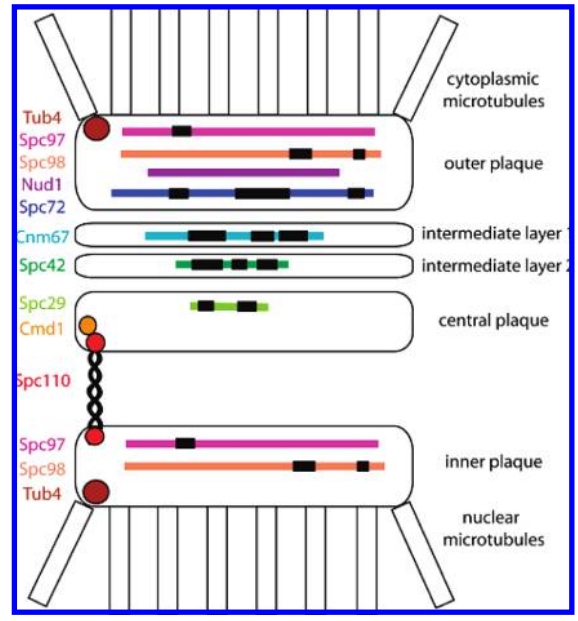

FIGURE 1: A schematic of the SPB core complex shows the protein composition and the layer(s) in which each component resides (*1, 6*). Proteins with known structures or structural properties (Tub4, Cmd1, and Spc110) are represented with shapes at the far left. Proteins of unknown structure are indicated with colored lines scaled to indicate protein length. Black bars indicate predicted coiled-coil regions. Membrane-associated and half-bridge proteins are not shown.

[†] This work was supported by NSF CAREER award MCB-0347203 and by the James H. Ferry Fund (MIT) and used the MIT Biophysical Instrumentation Facility for the Study of Complex Macromolecular Systems (NSF-0070319 and NIH GM68762).

[‡] Coordinates for the Spc42 coiled coil (2Q6Q) have been deposited in the RCSB Protein Data Bank.

* To whom correspondence should be directed. Tel: 617-452-3398. Fax: 617-253-4043. E-mail: keating@mit.edu.

[§] Present address: Department of Biochemistry, Albert Einstein College of Medicine, Bronx, NY 10461.

[1] Abbreviations: SPB, spindle pole body; EM, electron microscopy; PCR, polymerase chain reaction; IPTG, isopropyl β-D-thiogalactopyranoside; MALDI-TOF, matrix-assisted laser desorption/ionization−time of flight; MBP, maltose-binding protein; TCEP, tris(2-carboxyethyl)-phosphine hydrochloride; HPLC, high-performance liquid chromatography; CD, circular dichroism; T_m, melting temperature; FRET, fluorescence resonance energy transfer; TMAO, trimethylamine *N*-oxide; BS^3, bis(sulfosuccinimidyl) suberate; LRR, leucine-rich repeat; MRE, mean residue ellipticity.

10.1021/bi801378z CCC: $40.75
Published on Web 10/14/2008

Three-dimensional structural information is key to understanding the mechanism and function of important complexes such as the SPB. High-resolution structures are not available for the complex and are known for only three of the individual components: calmodulin (Cmd1) (*10*), γ-tubulin (Tub4) (*11*), and centrin (Cdc31) (*12*). A structure of Cdc31 in complex with part of component Sfi1 has also been reported (*13*). Interactions between SPB proteins have been determined using coimmunoprecipitation, genetic synthetic lethality, yeast two-hybrid assays, and FRET experiments (*1, 7, 14, 15*). For some SPB protein−protein interactions, the regions of interaction have been localized by disruption of interaction via point or deletion mutants (*1, 6*).

Most SPB proteins are predicted to contain one or more coiled-coil domains (*1, 7*). Coiled coils are a common structural motif, consisting of two or more α-helices wrapped around each other with a left-handed twist (*16*−*18*). Coiled-coil sequences exhibit a distinctive heptad pattern, [**abcdefg**]$_n$, that allows prediction of coiled-coil-forming regions using computer algorithms (*19*−*21*). The **a** and **d** positions are usually hydrophobic and pack into the coiled-coil interface. Coiled coils can associate intra- or intermolecularly, as homo- or heterooligomers, and in a parallel or antiparallel orientation. The motif often contributes to fiber formation or functions as an oligomerization or interaction domain. Coiled coils are common in cytoskeletal proteins, motor proteins, transcription factors, and membrane fusion proteins (*16, 22*).

Whether coiled-coil structures actually form within or between proteins of the SPB has not been confirmed experimentally. If present, they may serve to connect components through protein−protein interactions, either as homooligomers or heterooligomers, or serve as intramolecular structural features within individual components. In this study, we computationally identified and experimentally isolated predicted coiled-coil regions of SPB proteins and tested whether and how they interact. Coiled coils often retain their ability to fold when isolated from a larger protein context (*23, 24*). We focused on the 10 core proteins of the SPB complex in this study. These proteins are the most likely to interact, based on their close proximity within the complex and prior evidence supporting protein−protein interactions among them. We characterized four strongly associating coiled-coil homooligomers. Our data also support the possible significance of five weakly associating homooligomers and two heterooligomers. The high-resolution structure of a coiled-coil homodimer from Spc42 corroborates our solution assays and contributes to atomic resolution data describing the SPB.

MATERIALS AND METHODS

Coiled-Coil Prediction. Coiled-coil regions were identified in SPB protein sequences using Paircoil2 (*25*) with a *P* score cutoff of 0.96 and a 28-residue window (Figure 1 and Tables 1 and S1 in Supporting Information). Many of the regions were also high scoring according to the program Marcoil (*20*). Predicted coiled-coil regions were manually inspected, and N- and C-terminal ends were chosen based on a sharp drop in score (often at a Pro or Gly residue), a shift in register, and/or a *P* score of ≤0.93 (often corresponding to the loss of the hydrophobic/hydrophilic patterning). The first and last residues were chosen to occupy predicted **b**, **c**, or **f** positions, with the intent of directing linker sequences away from the coiled-coil interface. Because more than one coiled-coil region was predicted in some proteins, all peptides were named by appending "_#" after the protein name, where # designates the order of the detected coiled coil in the N- to C-terminal direction. Predictions for Cnm67 were ambiguous with respect to whether there may be one long coiled coil (Cnm67_2) or two shorter coiled coils (Cnm67_3 and Cnm67_4) in this protein; constructs accounting for both possibilities were tested (Figure S1 in Supporting Information). Multicoil was used to predict whether each coiled-coil region was more likely to form a dimer or a trimer (*26*).

Table 1: Predicted Coiled-Coil Regions of Core SPB Protein Sequences

coiled-coil name	systematic name	beginning residue	ending residue	Paircoil2 *P* score	dimer probability[a]	trimer probability[a]
Cnm67_1	YNL225c	159	263	1.00	**0.666**	0.252
Cnm67_2	YNL225c	303	461	1.00	**0.952**	0.496
Cnm67_3	YNL225c	303	384	1.00	**0.952**	0.496
Cnm67_4	YNL225c	369	461	1.00	**0.898**	0.173
Spc29_1	YPL124w	7	45	0.99	**0.477**	0.098
Spc29_2	YPL124w	129	174	1.00	0.094	**0.246**
Spc42_1	YKL042w	53	137	1.00	**0.946**	0.492
Spc42_2	YKL042w	178	213	0.99	0.002	**0.032**
Spc42_3	YKL042w	246	315	0.99	0.017	**0.068**
Spc72_1	YAL047c	97	160	1.00	0.235	**0.428**
Spc72_2	YAL047c	306	469	1.00	0.268	**0.389**
Spc72_3	YAL047c	568	622	1.00	**0.464**	0.228
Spc97	YHR172w	171	234	0.98	0.001	**0.032**
Spc98_1	YNL126w	622	690	0.97	0.001	**0.029**
Spc98_2	YNL126w	789	832	0.97	0.000	**0.005**

[a] Determined using Multicoil (*26*). The higher probability, indicating the predicted oligomer, is in bold.

Domain Annotation. Existing computational methods were used to annotate protein domains, folds, and motifs in SPB proteins. The following programs were run using default settings: mGenThreader (*27*) (only confidence levels of *certain* or *highly probable* were considered), DOMAC (*28*), and InterProScan (*29*).

Protein Production. Coding sequences corresponding to the individual coiled-coil regions of each SPB protein were generated using oligonucleotide assembly by PCR, with codons optimized for expression in *Escherichia coli* (*30*). Synthetic genes were ligated into a modified pET43a vector (Novagen) that contained the coding sequence for a His_6 tag for purification, a Flag tag for solubility, a tyrosine for detection by absorbance at 280 nm, and a cysteine at either the N- or C-terminus for differential labeling (Table S1 in Supporting Information). The sole native cysteine among all predicted coiled coils (Spc98_1 position 655, predicted coiled-coil heptad position **b**) was mutated to a serine. Plasmids were transformed into *E. coli* BB101 or BL21 cells (*31*). Expression of proteins was induced with 1 mM IPTG at OD_{600} = 0.4−0.6 for 4 h. Proteins were purified from cell lysate in 6 M guanidine hydrochloride with NiNTA resin (Qiagen), eluted with 60% acetonitrile and 0.1% trifluoroacetic acid, lyophilized, and stored at 4 °C. Protein concentrations were determined using the method of Edelhoch (*32*). Protein purity was greater than 90−95% by SDS−PAGE. The molecular weights of the proteins were verified by MALDI-TOF spectrometry to 0.1% accuracy.

For cross-linking experiments, synthetic genes were ligated into pSV282 (Vanderbilt University Medical Center, Center for Structural Biology) containing coding sequences for a His_6 tag, maltose binding protein (MBP), and a TEV cleavage

site. Plasmids were transformed into *E. coli* BL21 cells (*31*). Expression of proteins was induced with 1 mM IPTG at $OD_{600} = 0.4-0.6$ for 4 h. Proteins were purified under native conditions with NiNTA resin (Qiagen), dialyzed into 50 mM sodium phosphate and 150 mM NaCl, pH 7, and stored at −80 °C.

For crystallization, *S. cerevisiae* DNA encoding residues 65−138 from Spc42 was amplified by PCR and ligated into the expression vector pAED4 (*33*). The resulting plasmids were transformed into *E. coli* BL21 pLysS cells (*30*). Expression of proteins was induced with 0.4 mM IPTG at $OD_{600} = 0.4$ for 2 h. Proteins were purified in 8 M urea on a Sephadex G-50 size exclusion column (Pharmacia) and subsequently by reverse-phase HPLC (Vydac C18 column) (*39*).

Unique cysteines were reacted with either iodoacetamide (Sigma), fluorescein-5-maleimide (Invitrogen), or Alexa 568-maleimide (Invitrogen). Lyophilized proteins were resuspended at 100 μM in 50 mM Tris-HCl, 150 mM NaCl, and 5 M guanidine hydrochloride, pH 7.5, reduced with 1 mM TCEP, and incubated with 10−1000-fold excess conjugating molecule for 2−4 h. Alkylated proteins were separated from nonalkylated proteins and free iodoacetamide by reverse-phase HPLC (Vydac C18 column). Fluorophore-labeled proteins were desalted to remove free dye. Labeling efficiency was 80−90% based on SDS−PAGE and analytical reverse-phase HPLC analysis.

Circular Dichroism Spectroscopy. Alkylated proteins were analyzed at 15−50 μM in 50 mM sodium phosphate and 150 mM NaCl, pH 7. Circular dichroism (CD) spectra were measured from 195 to 280 nm in 1 nm increments with 2 s averaging time at 25 °C and/or 4 °C, in triplicate, using an Aviv model 400 CD spectrophotometer with a 0.1 cm cell.

For proteins with detectable secondary structure, thermal denaturation curves were measured at 1.5−5 μM in 50 mM sodium phosphate and 150 mM NaCl, pH 7, in a 1 cm cell with stirring. Thermal melts were measured at 222 nm from 4 to 50−90 °C in 2 °C increments with 60 s equilibrium time and 30 s averaging time, and refolding was measured by cooling to 4 °C at the same rate. Temperatures for 50% thermal denaturation (T_m values) were approximated as the midpoint between fits to linear folded and unfolded baselines. In the absence of a lower baseline, the signal at the lowest temperature was used to approximate the value of a constant folded baseline, and an upper limit for the T_m is reported. The same T_m values were obtained within 1 °C whether increasing or decreasing temperature, indicating reversible unfolding and adequate equilibration.

Fluorescence Resonance Energy Transfer (FRET) Assay. Proteins labeled with fluorescein or Alexa 568 were assayed alone or mixed in pairs in triplicate at 5−10 μM in 50 mM Tris-HCl, 150 mM NaCl, and 1 M guanidine hydrochloride, pH 7.5. Samples were prepared and mixed at 10-fold higher concentrations in 5 M guanidine hydrochloride and then diluted. Samples were incubated in wells of black 96-well plates for 1 h at 25 °C. Fluorescence was measured with a Perkin-Elmer Victor3 fluorescence plate reader at two different excitation and emission wavelengths: donor channel, excite 490 nm and emit 535 nm, and FRET channel, excite 490 nm and emit 615 nm. The FRET signal was corrected and normalized with the formula (*34*), $FRET = (Fm - Fa - Fd(Dm/Dd))/Dm$, where D = donor channel, F = FRET channel, a = acceptor sample alone (Alexa 568-labeled), d = donor sample alone (fluorescein-labeled), and m = mix of donor and acceptor samples, and averaged over three independent assays. Fluorescence was also measured after incubating the samples for 1 h at 4 °C and after the addition of 0.4 M trimethylamine *N*-oxide (TMAO), both at 25 and 4 °C. Control coiled coils (cJun, Fra1, Fos, Creb3, and cortexillin) were included in each assay to provide consistency (Figure S2 in Supporting Information).

Analytical Ultracentrifugation. Alkylated proteins were dialyzed against reference buffer (50 mM sodium phosphate and 150 mM NaCl, pH 7) and prepared at three concentrations each. Sedimentation equilibrium samples were spun in a Beckman XL-I analytical ultracentrifuge at 4 °C for 10−18 h (until equilibrated, as assessed by differences between sequential scans) at 20000, 25000, and 38000 rpm. Concentration was monitored by absorbance at 220−230 nm. Data were analyzed globally with the programs Ultrascan (*35*) and Heteroanalysis (*36*). Sedimentation velocity samples were spun at 20 °C for 12 h at 42000 rpm. Concentration was monitored by interference. Data were analyzed globally with the program Sedanal (*37*). Sednterp was used to calculate partial specific volumes from the amino acid sequences and solvent density from its composition (*38*).

Cross-Linking. Alkylated proteins were resuspended at 50 μM in 50 mM sodium phosphate and 150 mM NaCl, pH 7. MBP-fused proteins were used at 25 μM in 50 mM sodium phosphate and 150 mM NaCl, pH 7. Proteins were assayed alone or mixed in pairs, at 40 μM for alkylated proteins or 5 μM for MBP-fused proteins, and incubated 4 h at 25 °C after 5 min at 50 °C. Bis(sulfosuccinimidyl) suberate (BS^3) (Pierce) was added to a final concentration of 0.5 mM to the protein samples, incubated for 10 min, and quenched with 100 mM Tris-HCl, pH 8.0. Samples were analyzed by SDS−PAGE.

Crystallization. Two crystal forms of Spc42_1 (Table 3) were obtained at ambient temperature using the hanging-drop vapor diffusion method (*39*). For crystal form I, 1 μL of a 10 mg/mL protein solution in 10 mM phosphate, pH 8.0, was mixed with 1 μL of reservoir solution containing 100 mM Tris-HCl, pH 8.0, 200 mM $MgCl_2$, and 25% PEG 4000 and equilibrated against 500 μL of reservoir solution for several weeks. Crystal form II was grown using a similar approach but with reservoir solution containing 100 mM Tris-HCl, pH 8.25, 200 mM $CoCl_2$, and 25% PEG 3350. Crystals were taken directly from the crystallization drop and flash-frozen in a stream of cold nitrogen (X-stream cryogenic crystal cooler; Molecular Structure Corp.).

Structure Determination. Diffraction data were collected at the X4A beamline at Brookhaven National Laboratories, indexed using DENZO, and scaled with SCALEPACK (*40*). Initial phases were determined by molecular replacement using the program AMoRe (*41*) and a search molecule constructed by placing two copies of GCN4-p1 head-to-tail to yield an ~60-residue parallel dimer (*39, 42*). All side chains were truncated to serine. The correct side chains were built into the model using O and COOT as electron density became apparent during refinement with CNS (*39, 43−45*). Refinement included rounds of simulated annealing, positional refinement, and individual *B* factor refinement, as well as model rebuilding using O. Bulk solvent and anisotropic *B* factor corrections were applied throughout the refinement.

High anisotropy of the diffraction data was modified with ellipsoidal truncation and anisotropic scaling using the Diffraction Anisotropy Server (*46*). TLS refinement with Refmac (*47*) was used to improve final statistics (Table 3). We attempted to improve refinement by testing for the possible influence of twinning using the programs DETWIN, ZANUDA, and the UCLA twinning server (*41, 48, 49*), but the statistics did not improve. The final models were checked for potential model bias using simulated omit maps calculated with CNS. Graphics were made using PyMOL (*50*) (Figure 5). The structure contains two chains, A and B, corresponding to residues 66−129 and 67−132 of Spc42p, respectively; 119 water molecules are included. The model exhibits good geometry as determined by PROCHECK (*51*), with bond lengths and angles within the expected ranges. The Spc42_1 structures in the two crystal forms are very similar (RMSD between Cα atoms is 0.9 Å), although structural superposition reveals slightly different overall bending due to slightly different crystal contacts. Structural differences occur mainly on the surfaces of the two crystal variants, whereas the cores are virtually identical. Because data collected from the crystal of form II have higher resolution and the corresponding structure has better refinement statistics, we refer to crystal form II in all further discussions, and this is the form deposited in the PDB (2Q6Q).

RESULTS

Many Coiled Coils, but Few Other Domains, Are Predicted in Core SPB Protein Sequences. Although many coiled coils had been predicted in SPB proteins previously (*1, 7*), we used the updated program Paircoil2 to identify the locations of putative coiled coils within the core SPB protein sequences. Paircoil2 is a version of Paircoil with improved accuracy and sensitivity (*19, 25*). All but one of the core SPB proteins were predicted to contain one or more coiled-coil regions at the cutoff used. A total of 15 coiled-coil regions, ranging in length from 32 to 174 amino acids, were selected for experimental testing (Figure 1 and Tables 1 and S1 in Supporting Information).

Very few domains or structures other than coiled coils were predicted by a variety of domain- and fold-recognition programs. Tub4 was predicted to have a tubulin fold as expected, given that the structure of the human homologue, γ-tubulin, has been solved (*11*). The only other protein that was confidently annotated with domains and/or structures other than coiled coils was Nud1. The C-terminal half of Nud1 was predicted to adopt a leucine-rich repeat (LRR) structure. LRR domains are made of repeated structural units of α-helices and β-strands and are involved in protein−protein recognition (*52*). These domains may be important for assembling the SPB complex structure.

Several Core SPB Coiled Coils Self-Associate. Among 18 predicted coiled-coil regions in the SPB core proteins, we analyzed 15 as recombinant peptides using CD and a FRET assay. We excluded Spc110 because it was predicted to contain one long coiled coil (~650 residues) that has already been shown to act as a structural support between the inner and central layers and is highly likely to be a parallel homooligomer (*14, 53*). Paircoil2 predicted a coiled coil in each of Tub4 and Cmd1. These regions mapped to surface helices and did not form coiled coils in available crystal structures and thus were not characterized (*10, 11*).

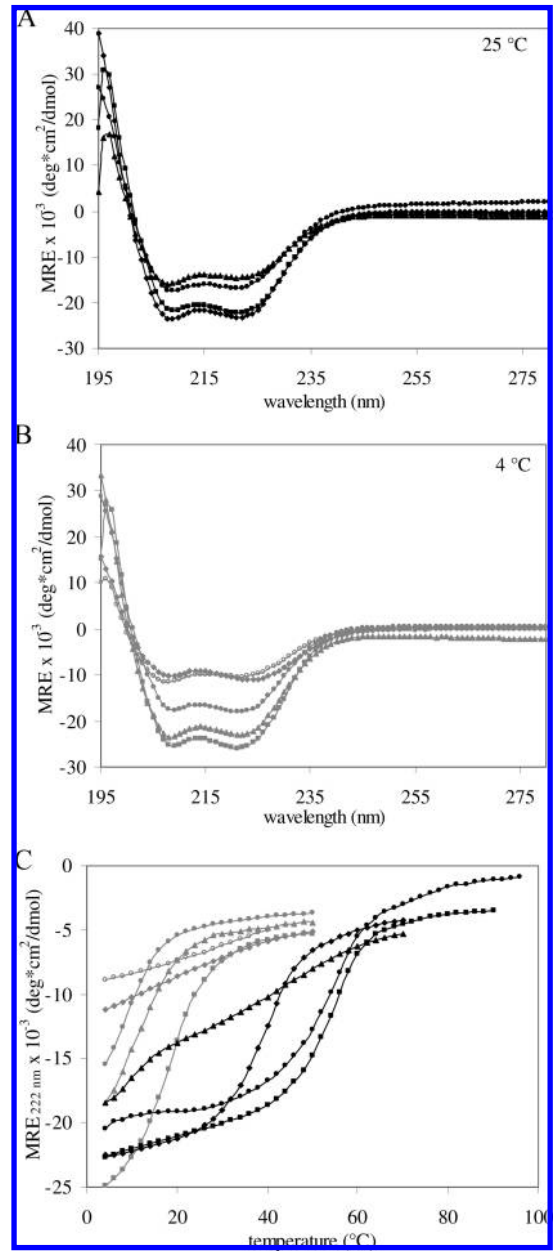

FIGURE 2: (A) CD spectra for strongly self-associating SPB coiled coils at 25 °C. Protein concentrations: Spc29_2 (●) 33 μM, Spc42_1 (■) 28 μM, Spc72_1 (▲) 47 μM, and Spc72_3 (◆) 28 μM. (B) CD spectra for weakly self-associating SPB coiled coils at 4 °C. Protein concentrations: Cnm67_1 (shaded circles) 32 μM, Cnm67_2 (shaded boxes) 32 μM, Cnm67_3 (shaded triangles) 23 μM, Spc72_2 (shaded diamonds) 15 μM, and Spc97 (open circles) 15 μM. (C) Thermal denaturation of self-associating SPB coiled coils monitored at 222 nm. Samples were diluted 1:10 from panels A and B in 50 mM sodium phosphate and 150 mM NaCl, pH 7. Symbols are as in panels A and B. MRE indicates mean residue ellipticity.

Coiled coils fold and interact cooperatively and exhibit α-helical CD spectra, often with approximately equal minima at 208 and 222 nm. Four SPB peptides, Spc29_2, Spc42_1, Spc72_1, and Spc72_3, met this criterion, with helical content ranging from ~40 to 60% at 25 °C as calculated based on the ellipticity at 222 nm (Figure 2A and Table 2) (*54*). Approximately 25−35% of each protein sequence consisted of extra amino acids (tags and linkers) not expected to form α-helical structure. Melting temperatures (T_ms) were determined for the proteins that folded cooperatively:

Table 2: Summary of Biophysical Analyses of Strongly Self-Associating, Weakly Self-Associating, and Weakly Heteroassociating Coiled Coils of the SPB Core Proteins

class	coiled coil	helical content (%)[a,b]	T_m (°C)[b]	helix orientation	expected MW for 1, 2, or 3 helices[c]	observed MW[d]
strong	Spc29_2	44 [59]	52	ambiguous	8289, 16578, 24867	24900, 25000[e]
	Spc42_1	57 [71]	53	parallel	13245, 26490, 39735	24800
	Spc72_1	38 [48]	noncooperative	ambiguous	10299, 20598, 30897	15300
	Spc72_3	61 [79]	39	parallel	9555, 19110, 28665	17400
weak	Cnm67_1	47 [55]	<11	parallel[d]		ND
	Cnm67_2	66 [75]	<19	parallel[d]		ND
	Cnm67_3	60 [74]	<13	parallel[d]		ND
	Spc72_2	28 [32]	noncooperative	ambiguous		ND
	Spc97	27 [35]	noncooperative	ambiguous		ND
hetero	Spc72_1-Spc97	ND	ND	ambiguous		ND
	Spc72_1-Spc72_2	ND	ND	ambiguous		ND

[a] Calculated based on ellipticity at 222 nm at 25 °C for strong complexes and 4 °C for weak complexes (*54*); values in brackets correspond to helicity of the SPB-derived portion of the peptide, assuming tags and linkers are not helical. [b] ND, not determined. [c] Weight(s) closest to the observed weight is (are) underlined. [d] Based on modest differences (Figures 3B and S3 and S4 in Supporting Information). [e] The two values correspond to the trimer MW that results from fitting a monomer−trimer equilibrium model to the data. The first value is from sedimentation equilibrium, and the second value is from sedimentation velocity.

Table 3: Data Processing and Refinement Statistics for Spc42_1

	I	II
crystal form		
space group	$P2_12_12_1$	$P2_12_12_1$
cell dimensions *a*, *b*, *c* (Å)	40.44, 55.89, 59.80	42.86, 57.79, 57.17
$\alpha = \beta = \gamma$ (deg)	90	90
resolution (Å)	20.0−2.2	20.0−1.97
R_{merge}[a]	0.067	0.075
$I/\sigma(I)$	14.0	8.2
all atoms/waters	1209/119	1192/119
multiplicity	5.0	4.5
completeness (%)	98.2	94.7
unique reflections (working/free)	6938/336	9799/475
R_{cryst}/R_{free}[b]	0.212/0.344	0.212/0.297
average *B* factor (Å^2)	31.50	36.77
RMSD from ideal values		
bond lengths (Å)	0.019	0.019
bond angles (deg)	1.77	1.91

[a] $R_{merge} = \sum\sum_j|I_j - \langle I\rangle|/\sum\sum|\langle I\rangle|$, where I_j is the intensity measurement for reflection *j* and $\langle I\rangle$ is the mean intensity for multiple recorded reflections. [b] $R_{cryst}/R_{free} = \sum||F_o| - |F_c||/\sum|F_o|$, where the crystallographic and free *R* factors are calculated using the working and test reflection sets, respectively. The test reflections included 10% of the total reflections that were chosen before refinement of the initial model and were not used during refinement.

Spc29_2 (52 °C), Spc42_1 (53 °C), and Spc72_3 (39 °C) (Figure 2C and Table 2). Spc72_1 showed gradual, noncooperative loss of helical structure with increasing temperature. Self-association of these four coiled coils was also supported by significant FRET signal (Figures 3A and S3 in Supporting Information).

The remaining putative coiled coils did not self-associate at 25 °C, as indicated by random-coil-like spectra (data not shown). However, five peptides, Cnm67_1, Cnm67_2, Cnm67_3, Spc72_2, and Spc97, gave α-helical spectra at 4 °C (Figure 2B). Cnm67_1, Cnm67_2, and Cnm67_3 unfolded cooperatively upon heating, with estimated T_ms <11, <19, and <13 °C, respectively (Figure 2C and Table 2). Spc72_2 and Spc97 unfolding was noncooperative. Self-association of these five coiled coils was not observed in the FRET assay at 25 °C (Figures 3A and S3 in Supporting Information), but under more stabilizing conditions; i.e., at 4 °C and in the presence of TMAO to counteract guanidine hydrochloride, Spc72_2 and Spc97 showed robust FRET signal. Cnm67_1, Cnm67_2, Cnm67_3, and Spc42_2 consistently showed very weak evidence for self-association under these conditions (Figures 3 and S3 and S4 in Supporting Information).

Several Core SPB Coiled Coils Heteroassociate. In addition to mediating association between multiple copies of the same protein, coiled-coil helices could heteroassociate, either inter- or intramolecularly. Almost all possible pairwise combinations of predicted core SPB coiled coils were mixed and tested against each other in the FRET assay under a variety of conditions (Figures 3A and S3 in Supporting Information). Because of their location within the SPB, the putative coiled-coil regions of Spc97 and Spc98 were only tested against the Spc72-derived peptides (*9*) (Figure 1). Because each peptide was expressed independently with an N-terminal and a C-terminal cysteine, and then labeled separately with fluorescein-maleimide and Alexa 568-maleimide, confidence in the detected associations was gained by assaying multiple combinations of peptide pairs. Fluorescein-labeled Spc29_2, Spc72_1, and Spc72_2 interacted with multiple peptides, but the same interactions were not always observed for the Alexa-labeled constructs. Five pairs were observed to interact consistently, independent of which fluorophore they were labeled with. In decreasing order of FRET signal, they are Spc29_2:Spc72_1, Spc72_1:Spc97, Spc72_1:Spc72_2, Spc72_1:Spc98_1, and Spc97:Spc98_1.

We attempted further characterization to confirm the heteroassociations. CD spectra of potentially interacting components were compared before and after mixing, but no change in signal was detected (data not shown). However, at least one of the participants in each candidate heterocomplex also homoassociated, and this observation is consistent with stronger homoassociation relative to heteroassociation. Using a cross-linking assay, association of Spc72_1 with both Spc97 and Spc72_2 was detected with the bifunctional amine-reactive chemical BS^3 (Figure S5 in Supporting Information). Heteroassociation of Spc98_1 with Spc72_1 or Spc97 was not observed in cross-linking experiments (data not shown), but these pairs gave the weakest FRET signal of all putative heterocomplexes, and the cross-linking assay may be less sensitive than the FRET assay. Interaction of Spc29_2 and Spc72_1 was also not detected by cross-linking (Figure S5 in Supporting Information), despite strong FRET signal. We judged that the FRET signal was likely caused by nonspecific interactions of the fluorescein-labeled constructs. Thus, FRET and cross-linking support weak heteroassociation of Spc72_1:Spc97 and Spc72_1:Spc72_2 (Table 2) and possibly very weak heteroassociation of

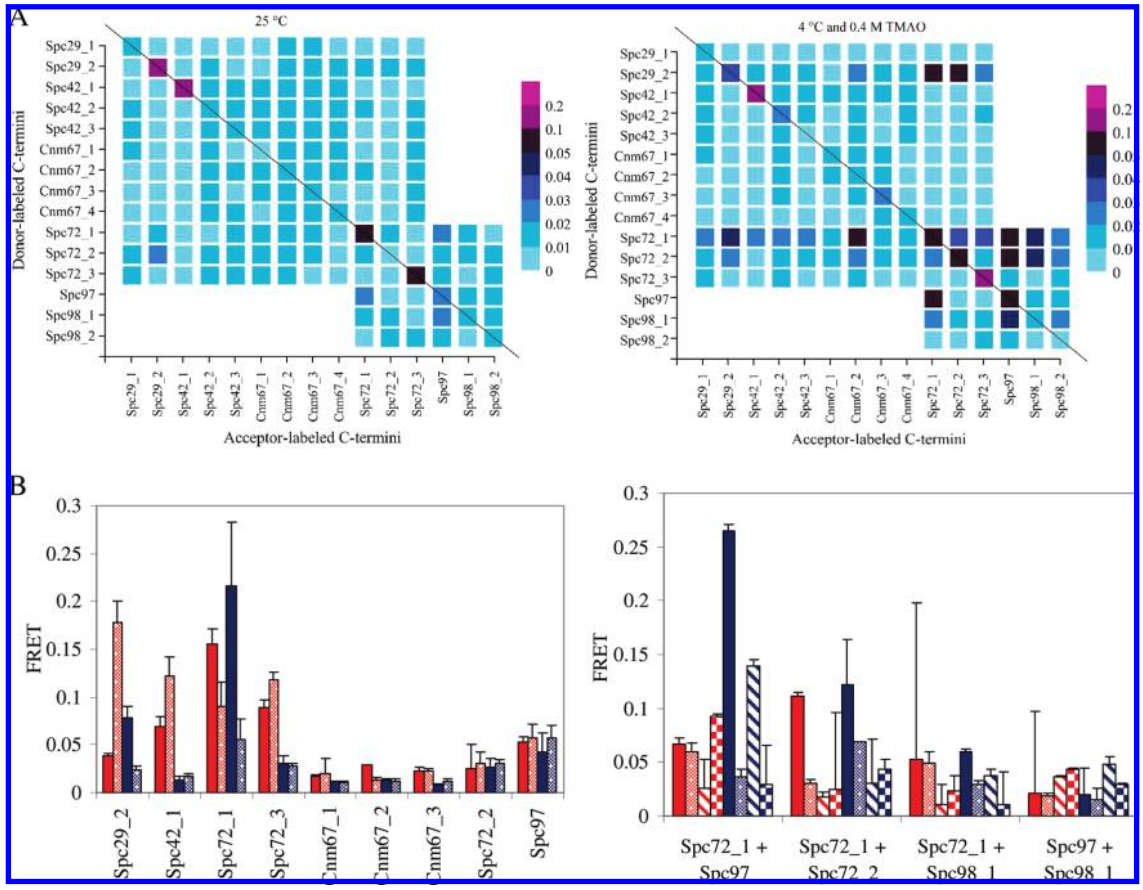

FIGURE 3: FRET assay of pairwise interactions. (A) FRET signal for mixtures of fluorophore-labeled SPB coiled coils. Alexa-labeled acceptors are in columns and fluorescein-labeled donors are in rows. Representative data shown are for acceptors and donors with labeled C-termini. Data at left were collected after incubating at 25 °C; data at right were collected after incubating at 4 °C with 0.4 M TMAO. Data from all conditions and for acceptors and donors with labeled N-termini are shown separately in Figure S3 in Supporting Information. (B) Orientation test for self-associating and heteroassociating SPB coiled coils. Representative data shown for strong self-associations were collected after incubating at 4 °C, and data shown for weak self-associations and heteroassociations were collected after incubating at 4 °C with 0.4 M TMAO. Data from all conditions are shown separately in Figure S4 in Supporting Information. Error bars represent the standard deviation of three independent assays. For homoassociations, four mixtures were tested for each protein, and results are shown from left to right: N-terminal donor + N-terminal acceptor (solid red), C-terminal donor + C-terminal acceptor (dotted red), N-terminal donor + C-terminal acceptor (solid blue), and C-terminal donor + N-terminal acceptor (dotted blue). For heteroassociations, eight mixtures were tested for each protein pair (A + B), and results are shown from left to right: N-terminal donor on A + N-terminal acceptor on B (solid red), C-terminal donor on A + C-terminal acceptor on B (dotted red), N-terminal donor on B + N-terminal acceptor on A (striped red), C-terminal donor on B + C-terminal acceptor on A (checkered red), N-terminal donor on A + C-terminal acceptor on B (solid blue), C-terminal donor on A + N-terminal acceptor on B (dotted blue), N-terminal donor on B + C-terminal acceptor on A (striped blue), and C-terminal donor on B + N-terminal acceptor on A (checkered blue). Red bars show combinations of coiled coils that bring fluorophores near each other in a parallel orientation, and blue bars show combinations of coiled coils that bring fluorophores near each other in an antiparallel orientation. Consistent results exhibiting clear orientation bias were obtained for Spc42_1 and Spc72_3, with weaker evidence for Cnm67_1, Cnm67_2, and Cnm67_3. All showed greater signal in the parallel orientation.

Spc72_1:Spc98_1 and Spc98_1:Spc97. The Spc29_2:Spc72_1 interaction is likely nonspecific.

Characterization of Core SPB Coiled-Coil Interactions. We determined the molecular weights of the strongly self-associating coiled coils using analytical ultracentrifugation. Sedimentation equilibrium data for both Spc42_1 and Spc72_3 fit well to single-species models, with observed molecular weights corresponding to those expected for dimers (Figure 4A and Table 2). Small deviations from the expected molecular weights have been observed previously with coiled coils (*55, 56*).

Sedimentation equilibrium and sedimentation velocity data for Spc29_2 gave observed molecular weights between those expected for a dimer and a trimer when fit to a single-species model (Figure 4B). However, both data sets fit to a monomer−trimer equilibrium model as well as they fit to a single-species model, giving observed molecular weights close to those expected (Table 2). Multicoil predicted Spc29_2 to be a trimer (Table 1), and cross-linking experiments also support trimerization (Figure S5 in Supporting Information).

Sedimentation velocity data for Spc72_1 gave observed molecular weights between those expected for a monomer and a dimer when fit to a single-species model (Figure 4B and Table 2). The data fit as well to a monomer−dimer model but gave unrealistic observed molecular weights corresponding to 0.75 of a monomer and 1.5 of a monomer. Although Spc72_1 was predicted by Multicoil to be a trimer (Table 1), cross-linking experiments showed significant dimer and no trimer (Figure S5 in Supporting Information). Concentration-dependent CD signal ruled out intramolecular interactions as the origin of helical signal (Figure S6 in Supporting Information). The lack of cooperativity in the thermal melt, evidence of aggregation under certain condi-

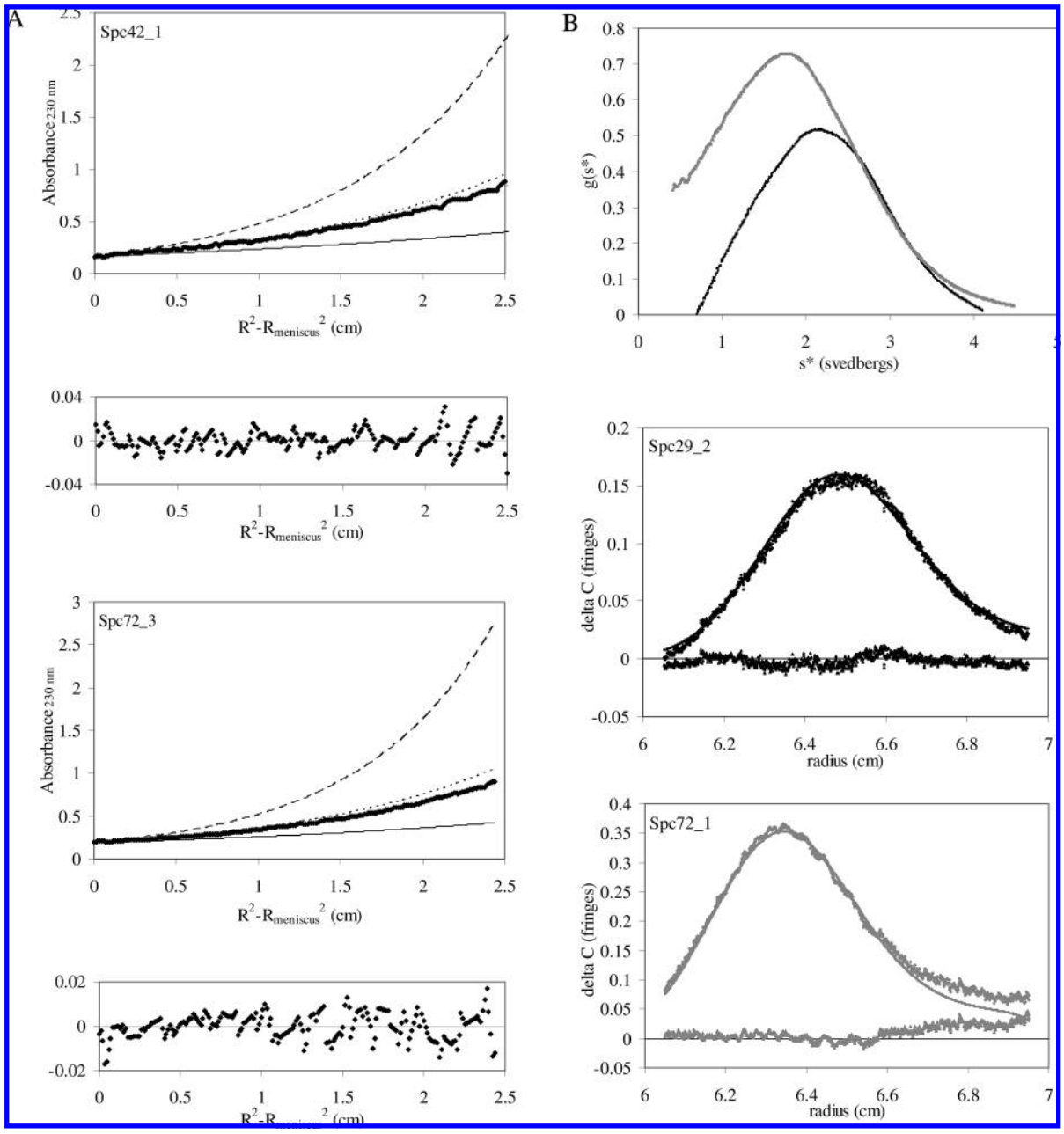

FIGURE 4: Characterization by analytical ultracentrifugation. (A) Sedimentation equilibrium data for Spc42_1 and Spc72_3. Data for three concentrations and three speeds were fit globally to a single-species model. A representative trace is shown, with residuals from the fit below. Curves expected for molecular weights corresponding to a monomer, dimer, or trimer are shown in solid, dotted, and dashed lines, respectively. (B) Sedimentation velocity data for Spc29_2 and Spc72_1. Data collected at three concentrations were analyzed by Sedanal and fit globally to a single-species model. Representative plots of sedimentation coefficient distributions and fitting of time-resolved concentration differences are shown at 50 μM for each protein. Spc29_2 is shown in black and Spc72_1 in gray with ♦ symbols representing observed data, lines representing fits, and residuals plotted around $y = 0$.

tions, and our observation of multiple heteroassociations by FRET and cross-linking assays suggest that Spc72_1 has a propensity toward self- and heteroassembly. But it may require the rest of the protein and/or complex to form the functionally appropriate associations.

The FRET assay was designed to distinguish the orientation of coiled-coil helices, in cases where this is unique and well-defined. Parallel coiled coils with fluorophores attached at the same termini were expected to generate more FRET signal than coiled coils with fluorophores on opposite ends. The reverse was expected for antiparallel dimers. Large differences in FRET were not expected for antiparallel trimers or tetramers. This assay was validated using parallel coiled-coil dimers of varying lengths (Figure S2 in Supporting Information). We measured the FRET signals for all possible pairwise combinations of labeled core SPB peptides (Figures 3B and S3 and S4 in Supporting Information). Self-associating SPB coiled coils Spc42_1 and Spc72_3 consistently exhibited significantly greater FRET when fluorophores were at the same ends of the helices, supporting a parallel orientation (Table 2). Cnm67_1, Cnm67_2, and Cnm67_3 also showed a weak preference for parallel orientation. The remaining self-associating SPB coiled coils and all heteroassociating SPB coiled coils were not consistently observed to give greater FRET with any labeling scheme. This could be because they interact as antiparallel

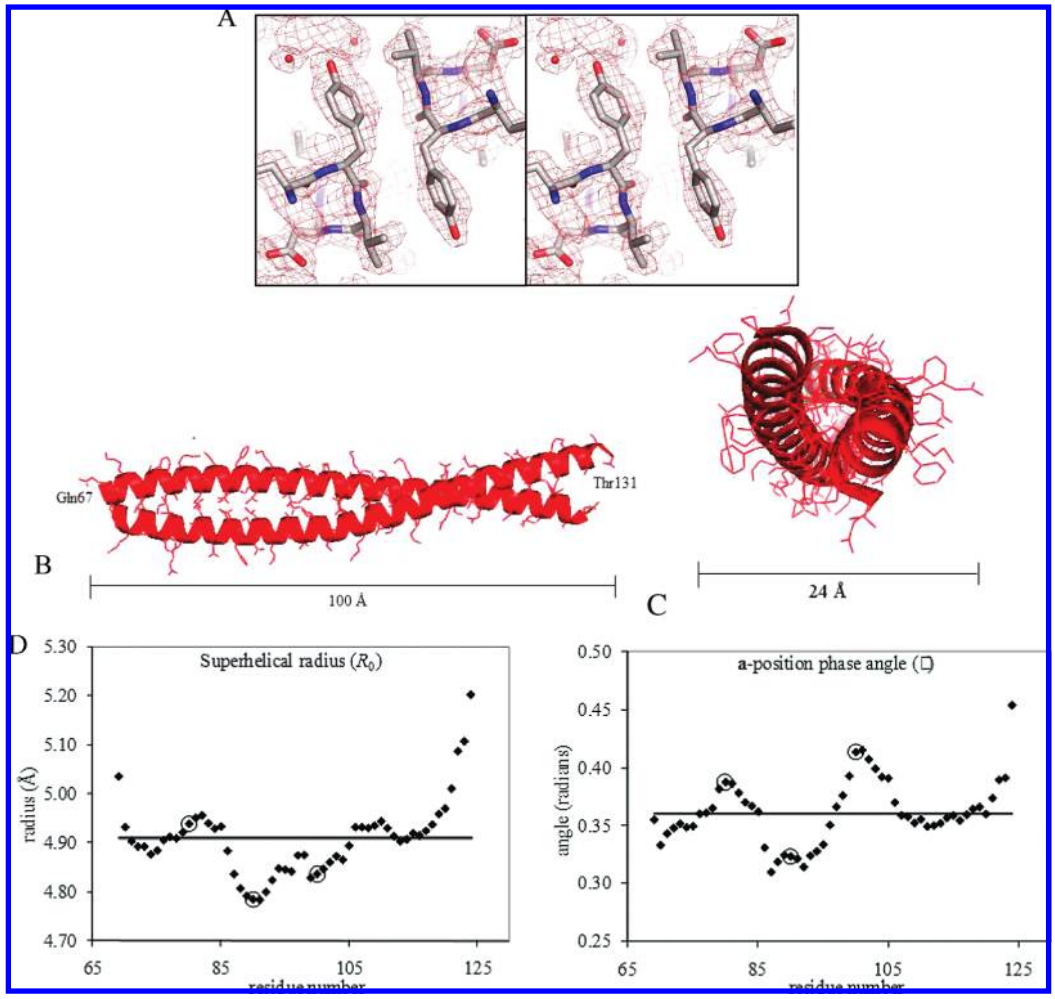

FIGURE 5: Crystal structure of Spc42_1. (A) Stereoview of the representative $2F_o - F_c$ electron density map near Tyr100 in the **d** position. Water molecules are shown as red spheres. (B) Side view. (C) Top view. The maximal diameter is approximately 24 Å with protrusion of side chains. (D) Fitted Crick parameters. The line shows the median value, and ♦ symbols show values fit using seven-residue windows centered on the indicated residue. Circled residues are Lys 79, Ala 90, and Tyr 100, discussed in the text.

trimers or tetramers, or in a staggered geometry, giving approximately equal FRET in either orientation. It could also be that these assemblies do not have a preference for a single orientation in the absence of the rest of the protein or complex. A third possibility is that the coiled coils were affected differentially by different combinations of fluorophores.

Crystal Structure of Spc42_1. Crystals of Spc42_1 belonged to space group $P2_12_12_1$ and contained one Spc42_1 homodimer in the asymmetric unit (*39*) (Table 3). Spc42_1 forms a parallel dimeric coiled coil (Figure 5), in agreement with the solution biophysical characterization and the predictions of Paircoil2 and Multicoil. Residues 67−128 of chain **A** and residues 67−131 of chain **B** were well defined in the electron density map. The length of the ordered part of Spc42_1 is ~100 Å, and the diameter of the Spc42_1 dimer is ~24 Å at its widest point (Cα−Cα distances are ~14 Å across the dimer). Residues at the core positions show canonical knobs-into-holes packing (*57*). Fitting Crick parameters for an idealized coiled coil to residues 67−128 of Spc42_1 gave a superhelical radius (R_0) of 4.91 Å, an **a**-position phase angle (ϕ) of 0.36 radians, and a superhelical frequency (ω_0) of −0.65 radians/amino acid (*57, 58*) (Figure 5D). The presence of a tyrosine (Tyr 100) in the **d** position of the fifth complete heptad is uncommon: only ~1.7% of **d**-position residues are Tyr in coiled coils of known structure that are longer than 21 residues (as judged by running the program SOCKET on recent releases of the PDB) (*56*). The crystal structure shows that the Cα−Cβ vectors of the tyrosine side chains from each helix point into the interface with perpendicular packing, as expected for **d**-position residues in parallel dimers (*58, 59*), but the hydroxyphenyl groups point out of the core toward the bulk solvent. This same geometry is observed for lysine residues (Lys 97) in **d** positions at the N-terminus of the coiled coil. In both cases, ϕ deviates locally to a higher value, as expected because the side chains would leave a gap in the core if the backbone did not compensate by bringing the **d** positions closer (Figure 5D). Other deviations of the Crick parameters include an expected decrease in R_0 and ϕ at Ala 90, an **a** position.

DISCUSSION

The structure of the SPB is not known at atomic resolution for numerous reasons. Because there are only 1−2 copies of the complex in each cell, obtaining sufficient sample to study is difficult. Purified complexes are heterogeneous in their dimensions and in the number of associated proteins, sometimes including microtubule-associated proteins (*7*). Reconstitution of recombinant components has been achieved for some subcomplexes of the SPB but not yet for the entire

complex (*60*). Even with a homogeneous SPB preparation, the enormous size and low symmetry of some layers would present crystallographic obstacles. Given these challenges, a strategy of breaking the complex into component parts, characterizing these parts individually, and ultimately assembling them into a larger model is an appealing alternative.

Over a decade of work has uncovered the identity of the protein components of the SPB and their approximate locations within the complex (*1, 6*−*9*). The structures of a few individual proteins or domains have been determined (*10*−*13*), and we now contribute the structure of a coiled-coil region of Spc42. Interactions between SPB components have been mapped at low resolution using yeast two-hybrid or immunoprecipitation approaches (*1, 6, 14, 15*). A recent study from the Davis laboratory devised a model of the central plaque based on *in vivo* FRET data (*14*). This model gave improved resolution because fluorescent probes were attached to either end of SPB proteins. Now we further refine aspects of the structure by demonstrating how some of the SPB proteins may interact, via coiled coils. We found many self-associations and few pairwise heteroassociations between coiled-coil regions of the core SPB proteins. These observations and subsequent biophysical characterization add to the constraints describing the molecular architecture of the SPB, as discussed below.

The large size of the SPB requires extensive oligomerization involving multiple copies of each protein. Thus, it is not surprising that the coiled coil, a very common oligomerization domain, is ubiquitous among proteins of the SPB. Coiled coils could play a role in SPB assembly by creating homo-oligomeric modules, by mediating interaction within a multiprotein module, or by linking distinct autonomous modules together. Our data suggest all types of roles. For example, strongly self-associating coiled coils in Spc29, Spc42, and Spc72 likely comprise subunits that may then assemble, via weaker self- or heteroassociating coiled coils or other interactions, into the larger complex. The weak interaction that we observed between Spc97 and Spc98_1 coiled coils may help to assemble the γ-tubulin complex, comprised of Tub4, Spc97, and Spc98. Attachment of the γ-tubulin complex to the rest of the outer plaque may involve the association of the Spc72_1 and Spc97 coiled coils. It is reasonable to assume that very weak interactions observed between isolated domains *in vitro* may nevertheless be functionally significant in the SPB. Local concentrations in the complex are very high, and avidity may play a large role.

Electron micrographs revealed that the central plaque of the SPB consists of a hexagonal lattice (*3*). Spc42 was sufficient to establish the framework of this lattice, based on its localization to the central plaque and the observation that its overexpression led to the formation of a lattice that extends outside the diameter of the SPB. Electron-dense features in the micrographs of Spc42 lie on a 3-fold axis, are ~25 Å in diameter, and have been interpreted as trimers or trimers of dimers (*3*). Our data support the latter model, also favored by Muller et al. (*14*). The trimer of dimers structure from HIV gp41 is ~35 Å in diameter (*61*), compatible with the low-resolution EM measurement. The available evidence thus leads to a model in which a homodimer formed via the first coiled-coil domain of Spc42 may further associate via a trimeric interface involving another part of the protein. This homotrimerization is probably not mediated by a coiled coil, given our observations that Spc42_2 and Spc42_3 do not self- or heteroassociate. Spc42 further associates with other proteins, potentially via coiled coils involving Spc42_2 and Spc42_3, to assemble the rest of the SPB complex.

The entire coiled-coil region of Cnm67 has been proposed to form a coiled-coil support separating intermediate layer 2 and the outer plaque, similar to the way the coiled-coil region of Spc110 separates the central and inner plaques (*53, 62*). Paircoil2 did not predict a continuous coiled coil but rather split the region into two or three individual coiled coils (Figure S1 in Supporting Information and Tables 1 and S1 in Supporting Information). A dramatic dip in score for over 25 residues, including helix-breaking prolines and a glycine and loss of the hydrophobic/hydrophilic patterning, led us to separate Cnm67 into three shorter sequences and test these in four peptides. However, our data are consistent with a parallel coiled-coil homooligomer that includes all of the regions tested serving a role as a spacer. We found that Cnm67_1, Cnm67_2, and Cnm67_3 each form a weak self-associating coiled coil and all three coiled coils showed evidence of parallel orientation (Figures 2 and 3). Multicoil also predicted a strong dimer preference for all three sequences (Table 1). This complex may be more stable in the context of the full-length Cnm67 protein or the SPB complex. The coiled-coil disrupting features detected by Paircoil2 could potentially have structural or functional consequences.

Although our data add to knowledge of the structure of the SPB, it is intriguing to speculate about the rest of the complex. Many of the predicted coiled-coil regions were not found to self- or heteroassociate. These sequences may not encode coiled coils, but that cannot be concluded from our data so far. Some coiled coils may require other parts of the protein to form. Weak coiled-coil interactions may not be detectable in our assays but could still be important in the high-density environment of the SPB. Further, only self-association and binary heteroassociation were tested here. Any coiled coils formed from three or more components would not be detected. The reagents that we have prepared are well suited for identifying a role for higher order coiled-coil assembly, and we are developing assays for that purpose. More work is also necessary to determine structures for non-coiled-coil regions and to address how these assemble into the SPB complex, although this is complicated by the lack of other predicted autonomous domains.

As additional data become available, characterized components can be incorporated into models describing the structural details of the SPB. The approach of assembling a model of the whole complex based on constraints derived from multiple data sources was pioneered for the SPB by Muller et al. (*14*). A similar strategy has recently been used on a larger scale by Sali and colleagues to construct a hybrid computational/experimental model for the nuclear pore complex (*63*). For the future, an approach of experimental dissection coupled with geometry-guided reassembly is a promising way of advancing our understanding of large protein complexes.

ACKNOWLEDGMENT

We thank J. R. S. Newman for work on the structure of Spc42_1 and P. S. Kim for support of the structural efforts,

E. de los Santos for bioinformatics support, K. N. Gutwin for coiled-coil residue frequencies, J. R. Apgar for coiled-coil parameter fitting, D. Pheasant, N. Olivier, and D. Hayes for analytical ultracentrifugation support, G. Roman for protein production support, and the Endy laboratory for use of equipment. We acknowledge members of the Keating laboratory and especially E. Fire, J. R. Apgar, A. W. Reinke, S. Dutta, K. H. Wang, J. Y. Hou, and J. R. S. Newman for comments on the work and the manuscript.

SUPPORTING INFORMATION AVAILABLE

Coiled-coil sequences, FRET data for control coiled coils, complete FRET data for core SPB coiled coils, and cross-linking data. This material is available free of charge via the Internet at http://pubs.acs.org.

REFERENCES

1. Jaspersen, S. L., and Winey, M. (2004) The budding yeast spindle pole body: structure, duplication, and function. *Annu. Rev. Cell Dev. Biol. 20*, 1–28.
2. Knop, M., Pereira, G., and Schiebel, E. (1999) Microtubule organization by the budding yeast spindle pole body. *Biol. Cell 91*, 291–304.
3. Bullitt, E., Rout, M. P., Kilmartin, J. V., and Akey, C. W. (1997) The yeast spindle pole body is assembled around a central crystal of Spc42p. *Cell 89*, 1077–1086.
4. Byers, B., and Goetsch, L. (1975) Behavior of spindles and spindle plaques in the cell cycle and conjugation of Saccharomyces cerevisiae. *J. Bacteriol. 124*, 511–523.
5. O'Toole, E. T., Winey, M., and McIntosh, J. R. (1999) High-voltage electron tomography of spindle pole bodies and early mitotic spindles in the yeast Saccharomyces cerevisiae. *Mol. Biol. Cell 10*, 2017–2031.
6. Helfant, A. H. (2002) Composition of the spindle pole body of Saccharomyces cerevisiae and the proteins involved in its duplication. *Curr. Genet. 40*, 291–310.
7. Wigge, P. A., Jensen, O. N., Holmes, S., Soues, S., Mann, M., and Kilmartin, J. V. (1998) Analysis of the Saccharomyces spindle pole by matrix-assisted laser desorption/ionization (MALDI) mass spectrometry. *J. Cell Biol. 141*, 967–977.
8. Winey, M., Baum, P., Goetsch, L., and Byers, B. (1991) Genetic determinants of spindle pole body duplication in budding yeast. *Cold Spring Harbor Symp. Quant. Biol. 56*, 705–708.
9. Adams, I. R., and Kilmartin, J. V. (1999) Localization of core spindle pole body (SPB) components during SPB duplication in Saccharomyces cerevisiae. *J. Cell Biol. 145*, 809–823.
10. Ishida, H., Takahashi, K., Nakashima, K., Kumaki, Y., Nakata, M., Hikichi, K., and Yazawa, M. (2000) Solution structures of the N-terminal domain of yeast calmodulin: Ca^{2+}-dependent conformational change and its functional implication. *Biochemistry 39*, 13660–13668.
11. Aldaz, H., Rice, L. M., Stearns, T., and Agard, D. A. (2005) Insights into microtubule nucleation from the crystal structure of human gamma-tubulin. *Nature 435*, 523–527.
12. Hu, H., and Chazin, W. J. (2003) Unique features in the C-terminal domain provide caltractin with target specificity. *J. Mol. Biol. 330*, 473–484.
13. Li, S., Sandercock, A. M., Conduit, P., Robinson, C. V., Williams, R. L., and Kilmartin, J. V. (2006) Structural role of Sfi1p-centrin filaments in budding yeast spindle pole body duplication. *J. Cell Biol. 173*, 867–877.
14. Muller, E. G., Snydsman, B. E., Novik, I., Hailey, D. W., Gestaut, D. R., Niemann, C. A., O'Toole, E. T., Giddings, T. H., Jr., Sundin, B. A., and Davis, T. N. (2005) The organization of the core proteins of the yeast spindle pole body. *Mol. Biol. Cell 16*, 3341–3352.
15. Rout, M. P., and Kilmartin, J. V. (1990) Components of the yeast spindle and spindle pole body. *J. Cell Biol. 111*, 1913–1927.
16. Burkhard, P., Strelkov, S. V., and Stetefeld, J. (2001) Coiled coils: a highly versatile protein folding motif. *Trends Cell Biol. 11*, 82–88.
17. Lupas, A. N., and Gruber, M. (2005) The structure of α-helical coiled coils. *Adv. Protein Chem. 70*, 37–78.
18. Mason, J. M., and Arndt, K. M. (2004) Coiled coil domains: stability, specificity, and biological implications. *ChemBioChem 5*, 170–176.
19. Berger, B., Wilson, D. B., Wolf, E., Tonchev, T., Milla, M., and Kim, P. S. (1995) Predicting coiled coils by use of pairwise residue correlations. *Proc. Natl. Acad. Sci. U.S.A. 92*, 8259–8263.
20. Delorenzi, M., and Speed, T. (2002) An HMM model for coiled-coil domains and a comparison with PSSM-based predictions. *Bioinformatics 18*, 617–625.
21. Lupas, A., vanDyke, M., and Stock, J. (1991) Predicting coiled coils from protein sequences. *Science 252*, 1162–1164.
22. Rose, A., and Meier, I. (2004) Scaffolds, levers, rods and springs: diverse cellular functions of long coiled-coil proteins. *Cell. Mol. Life Sci. 61*, 1996–2009.
23. Lumb, K. J., Carr, C. M., and Kim, P. S. (1994) Subdomain folding of the coiled coil leucine zipper from the bZIP transcriptional activator GCN4. *Biochemistry 33*, 7361–7267.
24. Oakley, M. G., and Kim, P. S. (1997) Protein dissection of the antiparallel coiled coil from Escherichia coli seryl tRNA synthetase. *Biochemistry 36*, 2544–2549.
25. McDonnell, A. V., Jiang, T., Keating, A. E., and Berger, B. (2006) Paircoil2: improved prediction of coiled coils from sequence. *Bioinformatics 22*, 356–358.
26. Wolf, E., Kim, P. S., and Berger, B. (1997) MultiCoil: a program for predicting two- and three-stranded coiled coils. *Protein Sci. 6*, 1179–1189.
27. McGuffin, L. J., and Jones, D. T. (2003) Improvement of the GenTHREADER method for genomic fold recognition. *Bioinformatics 19*, 874–881.
28. Cheng, J. (2007) DOMAC: an accurate, hybrid protein domain prediction server. *Nucleic Acids Res. 35*, W354−W356.
29. Zdobnov, E. M., and Apweiler, R. (2001) InterProScan—an integration platform for the signature-recognition methods in InterPro. *Bioinformatics 17*, 847–848.
30. Hoover, D. M., and Lubkowski, J. (2002) DNAWorks: an automated method for designing oligonucleotides for PCR-based gene synthesis. *Nucleic Acids Res. 30*, e43.
31. Studier, F. W., Rosenberg, A. H., Dunn, J. J., and Dubendorff, J. W. (1990) Use of T7 RNA polymerase to direct expression of cloned genes. *Methods Enzymol. 185*, 60–89.
32. Edelhoch, H. (1967) Spectroscopic determination of tryptophan and tyrosine in proteins. *Biochemistry 6*, 1948–1954.
33. Doering, D. S. (1992) Ph.D. Thesis, Massachusetts Institute of Technology, Cambridge, MA.
34. Gordon, G. W., Berry, G., Liang, X. H., Levine, B., and Herman, B. (1998) Quantitative fluorescence resonance energy transfer measurements using fluorescence microscopy. *Biophys. J. 74*, 2702–2713.
35. Demeler, B. (2005) UltraScan A Comprehensive Data Analysis Software Package for Analytical Ultracentrifugation Experiments, in *Modern Analytical Ultracentrifugation: Techniques and Methods* (Scott, D. J., Harding, S. E., and Rowe, A. J., Eds.) pp 210−229, Royal Society of Chemistry, London, U.K.
36. Cole, J. L., and Lary, J. W. (2006)Heteroanalysis, Analytical Ultracentrifugation Facility, University of Connecticut, Storrs, CT.
37. Stafford, W. F., and Sherwood, P. J. (2004) Analysis of heterologous interacting systems by sedimentation velocity: curve fitting algorithms for estimation of sedimentation coefficients, equilibrium and kinetic constants. *Biophys. Chem. 108*, 231–243.
38. Philo, J. (2006)Sednterp, Alliance Protein Laboratories, Thousand Oaks, CA.
39. Newman, J. R. S. (2001) Ph.D. Thesis, Massachusetts Institute of Technology, Cambridge, MA.
40. Otwinowski, Z., and Minor, W. (1997) Processing of X-ray diffraction data collected in oscillation mode. *Methods Enzymol. 276*, 307–326.
41. The CCP4 suite: programs for protein crystallography (1994) *Acta Crystallogr., Sect. D: Biol. Crystallogr. 50*, 760−763.
42. O'Shea, E. K., Klemm, J. D., Kim, P. S., and Alber, T. (1991) X-ray structure of the GCN4 leucine zipper, a two-stranded, parallel coiled coil. *Science 254*, 539–544.
43. Brunger, A. T., Adams, P. D., Clore, G. M., DeLano, W. L., Gros, P., Grosse-Kunstleve, R. W., Jiang, J. S., Kuszewski, J., Nilges, M., Pannu, N. S., Read, R. J., Rice, L. M., Simonson, T., and Warren, G. L. (1998) Crystallography & NMR system: A new software suite for macromolecular structure determination. *Acta Crystallogr., Sect. D: Biol. Crystallogr. 54*, 905–921.

44. Emsley, P., and Cowtan, K. (2004) Coot: model-building tools for molecular graphics. *Acta Crystallogr., Sect. D: Biol. Crystallogr. 60*, 2126–2132.
45. Jones, T. A., Zou, J. Y., Cowan, S. W., and Kjeldgaard, M. (1991) Improved methods for building protein models in electron density maps and the location of errors in these models. *Acta Crystallogr. A 47* (Part 2), 110–119.
46. Strong, M., Sawaya, M. R., Wang, S., Phillips, M., Cascio, D., and Eisenberg, D. (2006) Toward the structural genomics of complexes: crystal structure of a PE/PPE protein complex from Mycobacterium tuberculosis. *Proc. Natl. Acad. Sci. U.S.A. 103*, 8060–8065.
47. Winn, M. D., Isupov, M. N., and Murshudov, G. N. (2001) Use of TLS parameters to model anisotropic displacements in macromolecular refinement. *Acta Crystallogr., Sect. D: Biol. Crystallogr. 57*, 122–133.
48. ZANUDA (http://www.ysbl.york.ac.uk/YSBLPrograms/).
49. Padilla, J., and Yeates, T. O. (2003) A statistic for local intensity differences: robustness to anisotropy and pseudo-centering and utility for detecting twinning. *Acta Crystallogr., Sect. D: Biol. Crystallogr. 59*, 1124–1130.
50. DeLano, W. L. The PyMOL Molecular Graphics System (http://pymol.sourceforge.net).
51. Morris, A. L., MacArthur, M. W., Hutchinson, E. G., and Thornton, J. M. (1992) Stereochemical quality of protein structure coordinates. *Proteins 12*, 345–364.
52. Kobe, B., and Kajava, A. V. (2001) The leucine-rich repeat as a protein recognition motif. *Curr. Opin. Struct. Biol. 11*, 725–732.
53. Kilmartin, J. V., Dyos, S. L., Kershaw, D., and Finch, J. T. (1993) A spacer protein in the Saccharomyces cerevisiae spindle poly body whose transcript is cell cycle-regulated. *J. Cell Biol. 123*, 1175–1184.
54. Chen, Y. H., Yang, J. T., and Chau, K. H. (1974) Determination of the helix and beta form of proteins in aqueous solution by circular dichroism. *Biochemistry 13*, 3350–3359.
55. Blacklow, S. C., Lu, M., and Kim, P. S. (1995) A trimeric subdomain of the simian immunodeficiency virus envelope glycoprotein. *Biochemistry 34*, 14955–14962.
56. Schnarr, N. A., and Kennan, A. J. (2003) Specific control of peptide assembly with combined hydrophilic and hydrophobic interfaces. *J. Am. Chem. Soc. 125*, 667–671.
57. Crick, F. H. (1953) The packing of α-helices: simple coiled coils. *Acta Crystallogr. 6*, 689–697.
58. Harbury, P. B., Tidor, B., and Kim, P. S. (1995) Repacking protein cores with backbone freedom: structure prediction for coiled coils. *Proc. Natl. Acad. Sci. U.S.A. 92*, 8408–8412.
59. Walshaw, J., and Woolfson, D. N. (2001) Socket: a program for identifying and analysing coiled-coil motifs within protein structures. *J. Mol. Biol. 307*, 1427–1450.
60. Vinh, D. B., Kern, J. W., Hancock, W. O., Howard, J., and Davis, T. N. (2002) Reconstitution and characterization of budding yeast gamma-tubulin complex. *Mol. Biol. Cell 13*, 1144–1157.
61. Chan, D. C., Fass, D., Berger, J. M., and Kim, P. S. (1997) Core structure of gp41 from the HIV envelope glycoprotein. *Cell 89*, 263–273.
62. Schaerer, F., Morgan, G., Winey, M., and Philippsen, P. (2001) Cnm67p is a spacer protein of the Saccharomyces cerevisiae spindle pole body outer plaque. *Mol. Biol. Cell 12*, 2519–2533.
63. Alber, F., Dokudovskaya, S., Veenhoff, L. M., Zhang, W., Kipper, J., Devos, D., Suprapto, A., Karni-Schmidt, O., Williams, R., Chait, B. T., Rout, M. P., and Sali, A. (2007) Determining the architectures of macromolecular assemblies. *Nature 450*, 683–694.

BI801378Z